Hindawi
Journal of Nanomaterials
Volume 2023, Article ID 3657314, 11 pages
https://doi.org/10.1155/2023/3657314

Research Article

Analytical and Neural Network Analysis on Flux-Coated Aluminium Alloy by Activated TIG Welding with Synthesized Nanocomposites

V. L. Raja,[1] A. M. Senthil Kumar,[2] K. Shantha Kumari,[3] R. Bharanidharan,[4] P. Ezhilarasi,[5] S. Rajeshkannan,[5] T. M. Nithya,[6] and S. Venkatesh Kumar[7]

[1]*Department of Mechanical Engineering, Loyola Institute of Technology, Palanchur, Chennai 600123, Tamil Nadu, India*
[2]*School of Computer Science and Engineering, Vellore Institute of Technology, Chennai 600127, Tamil Nadu, India*
[3]*Department of Data Science and Business Systems, School of Computing, SRM Institute of Science and Technology, Chennai 603203, Tamil Nadu, India*
[4]*Department of Electrical and Electronics Engineering, Karpagam Academy of Higher Education, Coimbatore 641021, Tamil Nadu, India*
[5]*Department of Electronics and Communication Engineering, St. Joseph's College of Engineering, OMR, Chennai 600119, Tamil Nadu, India*
[6]*Department of Computer Science and Engineering, K. Ramakrishnan College of Engineering, Trichy 621112, Tamil Nadu, India*
[7]*Department of Mechanical Engineering, College of Engineering and Technology, Mettu University, P.O. Box: 318, Mettu, Ethiopia*

Correspondence should be addressed to S. Venkatesh Kumar; s.venkateshkumar@meu.edu.et

Received 27 August 2022; Revised 11 December 2022; Accepted 25 January 2023; Published 20 February 2023

Academic Editor: Ridwan Yahaya

Copyright © 2023 V. L. Raja et al. This is an open access article distributed under the Creative Commons Attribution License, which permits unrestricted use, distribution, and reproduction in any medium, provided the original work is properly cited.

This research focused to synthesize the material by the tungsten inert gas (TIG) welding process with support of appropriate flux coating material. Therefore the required amount of flux coating material was utilized to enhance the mechanical properties of the specified localized welded regions. Hence, this study concentrated to select the nano-SiO_2 flux particles that were employed for TIG process. This activated TIG welding composes the flux-coated welding on the base metal of AA5083-H111, as this material was highly reactive with SiO_2 by the presence of magnesium precipitates and well synthesized after the welding. The post- and preheat treatment process was achieved before and after welding. The selection of activated TIG process parameters composed of strengthened weld specimens along with constant parameters like electrode tip angle and flow rate, respectively. Initially, the process parameters were designed by the statistical analysis of Box Behnken method with support of regression formulation to determine the optimal solution. The maximum tensile strength was attained at the welding process parameters of welding speed (100 mm/min), voltage (13 V), and current (125 amps). The higher hardness was achieved at the process parameters of welding speed (80 mm/min), voltage (12 V), and current (125 amps), respectively. Finally, the neural network approach was utilized to verify the predicted responses of tensile and microhardness properties. The interaction plots, mean plots, and 3D scatter plots were influenced to enhance the process parameters. In this research, mechanical properties were enhanced by the flux-coated SiO_2 and the analytical method also advances the optimal parameters.

1. Introduction

Over the years, various categories of welding have been utilized in various sectors of the industries [1]. But since welded joints could not properly accommodate with thermoplastic condition, the entire welding operations totally collapsed [2]. Different categories of welding are used in various mechanical industries [3]. Especially, tungsten inert gas (TIG) welding is used highly in these industries [4]. The TIG welding generates heat with ultimate support of electric arc with consumable tungsten electrodes to join various metals together [5]. TIG welding was initiated in 1942 by the scientist Russel; many researchers developed welding into the aluminum-based magnesium alloy [6]. Formerly, this type of material joint

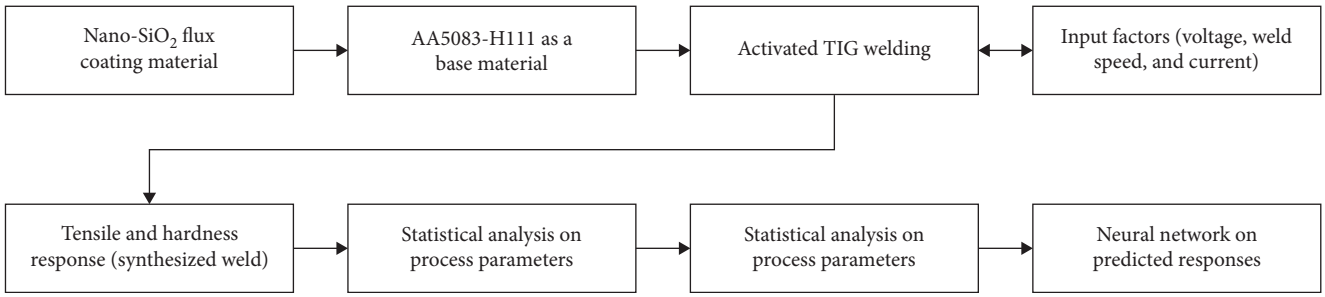

Figure 1: A-TIG-coated process layout.

was difficult to weld during the TIG process [7]. Nonferrous and ferrous materials are frequently joined together by TIG process [8].

At the same time, TIG welding was used where there were requirements to fulfill the quality and serious situations [9]. It has protected the weld pool by shielding gas, and this welding is easy to carry in any position, and fine soft welding was carried out. TIG welding works under the activated flux or without flux based on the applications. Meanwhile activated-flux-TIG welding is used where thicker welding is needed. This welding was used in various applications like, pipe, plate, casted plate or pipe, ship building, and aerospace sectors. Some of the minor limitations are accomplished in the TIG welding process [10].

During the single bead of weld on higher thickness materials, joint was not properly attained. Similarly, the edge preparation enhancements need more filler materials to pack the welds and the cost of operation was also high [11]. Plates exceeding 3 mm thickness needed more than one pass of TIG welding then only the joint efficiency was highly accomplished [12]. To improve the maximum thickness, the component should meet the necessity of lesser welding speed and multipass method and then will blend together [13]. After the completion of the process, additional cost was needed to clean the edges and maximum time was consumed to attain the full process [14]. Pavan et al. [15] presented the bead on plate TIG process with aiding of activated flux to stainless steel material. The design of experiments was used to measure the optimization of process parameters. Finally, the maximum density of welded specimens were achieved at bead on plate processed 316L stain less steel. Babbar et al. [16] investigated that the activated TIG welding on the multi-based flux materials were influenced on the stainless material. In this study, tensile strength and depths of penetrations were analyzed in detail. The current, voltage, and flow rates were highly utilized to enhance the process parameters. Moreover, most of the specimens achieved better mechanical characteristics in the welded joints. Sakthivel et al. [17] studied the activated TIG process on the 316L stainless steel material with maximum temperature at 923 K. The mechanical properties, like creep strength, were achieved at high on the welded area. At the same time cavitations also reduced. The characterization of the welded region provides better intermetallic phases. Muzamil et al. [18] synthesized the nanocarbon tubes, and titanium oxide flux-coated materials were incorporated on the AA6061 aluminium alloy. Addition of flux on AA6061 enhances its mechanical properties. Similarly, weld depths, distortions, and weld seams were analyzed on the welded region of AA6061. Vora and Badheka [19] presented the activated TIG on the steel with the utilization of ferritic material. The postweld treatment was achieved on all the welded samples for improving the mechanical properties. The flux-treated samples achieved better enhanced properties than the unprocessed materials. Above literature clearly define various activated TIG processes on various materials. But AA5083-H111 with nano-SiO_2 flux treating was not achieved fully. So this research concentrates to focus AA5083-H111 with constant weight fraction of nano-SiO_2-synthesized samples which were composed by the A-TIG welding. Wu et al. [20] investigated the TIG welded on the titanium alloy and analyzed the mechanical properties by various influence of frequency. The mechanical properties were improved by increasing the frequencies. At the same time, statistical and neural network combination was approached on the TIG-welded samples to analyze the optimal process parameters. Figure 1 shows the graphical layout for present investigation.

2. Material and Methods

In this TIG welding process, AA5083-H111 aluminium–magnesium alloy was utilized to conduct the joining process. Before the initiation of TIG process, base material could be engaged for heat treatment process. The two stages of preweld actions, that is, 850°C kept at 20 hr and 750°C kept at 18 hr were carried out on the selected base material. The uniform dispersion of strengthening particles was successfully carried out, and the required dimensions of the base plate were machined to 150 mm × 50 mm × 6 mm size from the purchased materials. Then 45° notch with V type was designed on the above dimension plate to fill the flux material. The nano-SiO_2 flux was coated on the selected base metal with support of carbinol mixing to attain regularity that looks like a paint material. Then the help of paint brush was taken to fulfill the 45° V notch gap.

The welding parameters are the most important aspect to attain complete welding. The welding parameters are welding speed (80–100 mm/min), voltage (12–14 V), and current (120–130 amps), respectively. These parameters composed better joints as stated by different researchers [21]. The butt joint configuration was completed through this TIG welding process with flux-coated material along the center portion of the base material. The 10 mg nano-SiO_2 flux was coated on

Table 1: Box Behnken-based design of welding parameters.

Std. order	Weld order	Pt. categories	Blocks	Welding speed (mm/min)	Voltage (V)	Current (amp)
14	1	0	1	90	13	125
10	2	2	1	90	14	120
2	3	2	1	100	12	125
3	4	2	1	80	14	125
13	5	0	1	90	13	125
7	6	2	1	80	13	130
5	7	2	1	80	13	120
9	8	2	1	90	12	120
4	9	2	1	100	14	125
8	10	2	1	100	13	130
6	11	2	1	100	13	120
11	12	2	1	90	12	130
12	13	2	1	90	14	130
15	14	0	1	90	13	125
1	15	2	1	80	12	125

the base material then the weld was produced or synthesized on the weldment region [21]. During the activated TIG welding process, 65° tip angle with 3% thorium-mixed electrode was used and flow rate of 13 L/min was maintained. During the postwelding process, temperature of 690°C was kept at 20 hr time period for all the specimens to mitigate the internal stresses [22]. Then the welded synthesized specimens were employed to conduct the mechanical testing and characterization examinations. After the postweld heat treatment process, all the welded samples were entered into the nondestructive tests for analyzing the defect-free surfaces. All the mechanical performances were conducted as per the ASTM system [23]. During the mechanical tests, tensile was prepared as per ASTM of E-09 and hardness was prepared as per the ASTM of E-384, respectively.

Prior to A-TIG welding on AA 5083-H111 base material, the process parameters are designed by the statistical method of response surface methodology. From the response method, Box Behnken technique was assigned the parameter levels with supporting of Minitab software [24]. Among the various optimization methods like grey relational, central composite design, desirability, and TOPSIS approach, Box Behnken method provides a better optimal solution by the increase of maximum necessity trial runs than the general factorial method. Overall 15 weld runs were accommodated to produce the butt weld on the base material of AA5083-H111. The design table of processing parameters is presented in Table 1.

3. Results and Discussion

After the postweld heat treatment was conducted, weld specimens were accounted into tensile and hardness strength experiment to analyze the mechanical potency of welded samples. As per the design of Box Behnken method, the entire weld runs were completed with activated flux-coated TIG welding. As per the ASTM systems of E-09 subcategories, tensile specimens were prepared. Similarly, hardness specimens were prepared and the standard dimension and the measurement values were taken on the nugget surface region by Vicker's hardness testing machine [25]. The entire weld specimens achieved better tensile properties and enhanced hardness strength than the as-cast raw base material. The base metal properties are 220 MPa and 74 Hv, respectively. Table 2 shows the overall mechanical properties of welded specimens. As per the recommendations of Box Behnken design, all 15 welded specimens were engaged to carry out the mechanical testing. The entire welded specimens achieved better mechanical properties when compared with base material. Figures 2 and 3 shows the tensile properties' and hardness strength's graphical representations. Those figures were plotted by the origin tools implementing the 5% error plots on the tensile and hardness bars. From Figure 2, it is understood that the sample 14 attained the maximum tensile properties when compared with other set of flux-coated samples. The 14th sample's parameters were 90 mm/min, 13 V, and 125 amps with respect to welding speed, voltage, and current. The nano-SiO_2 flux-coated sample was fully synthesized on the base material. Due to the presence of nano-SiO_2 the tensile properties and hardness strength enhances. At the same time, aluminum–magnesium alloy with nano-SiO_2 was synthesized during the single pass of the activated TIG welding technique.

The hardness portion of welded specimens achieved fine strength due to the presence of nano-SiO_2 flux material. Similarly, heat-affected zone strength was significantly less when compared with flux-coated zones due to the synthesized nanosilicon oxide particles dispersed uniformly on the AA5083-H111. At the same time, V notch groove successfully packed the nano-SiO_2 particles by the activated TIG welding process. Moderate welding speed and voltage with increment of welding current improves the weld strength, and evenly dispersed silicon oxide flux causes enhancement in the hardness properties in the weld zone.

Table 2: Mechanical properties of TIG-activated-flux-coated welded samples.

Weld order	Welding speed (mm/min)	Voltage (V)	Current (amp)	Tensile	Hardness
1	90	13	125	245	81
2	90	14	120	254	85
3	100	12	125	261	84
4	80	14	125	258	89
5	90	13	125	265	91
6	80	13	130	238	88
7	80	13	120	263	86
8	90	12	120	241	92
9	100	14	125	256	83
10	100	13	130	274	79
11	100	13	120	267	82
12	90	12	130	258	85
13	90	14	130	261	81
14	90	13	125	280	91
15	80	12	125	249	90

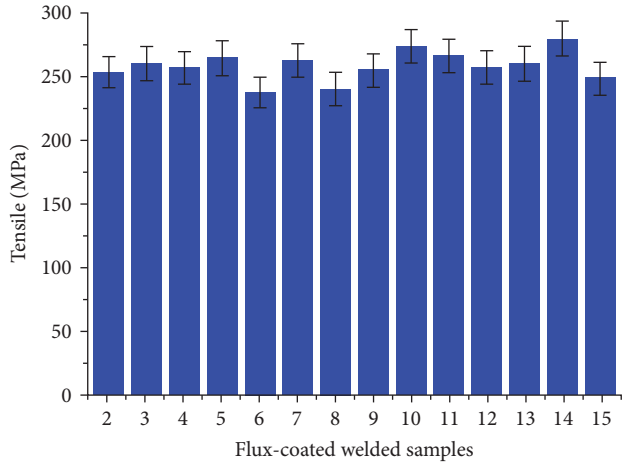

Figure 2: Tensile properties on the nano-SiO_2-flux-coated specimens.

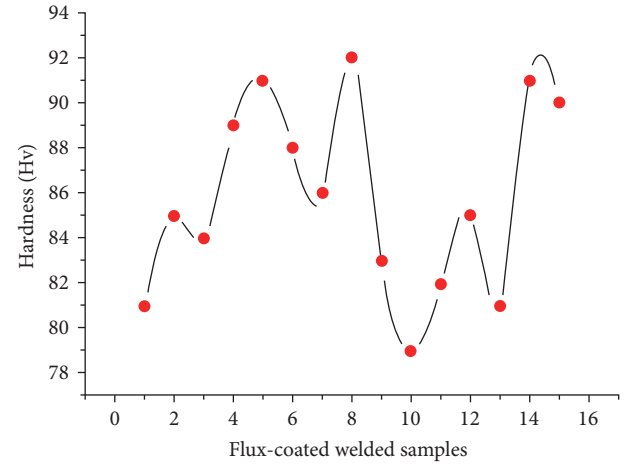

Figure 3: Hardness on the nano-SiO_2-flux-coated specimens.

3.1. Statistical Analysis of Activated TIG Welding Process Parameters. In this research, TIG-welded processing parameters were engaged into the statistical performance for improving the welding characteristics with respected outcomes. Therefore, response surface methodology was an appropriate technique to implement the welding characteristics. From the RSM method, Box Behnken method was used to analyze the processing parameters with effect various plots like histogram plots, Pareto charts, interaction plots, and main effect plos. These plots were used to enhance the outcomes with standardized effects. Regression equations create the model effectively with uncoded units for tensile response. The following equation shows the regression equation of tensile strength.

$$\begin{aligned}\text{Tensile strength} = {} & -2158 - 14.5\ \text{welding speed} + 283\ \text{voltage} + 18.9\ \text{current} \\ & - 0.0017\ \text{welding speed} \times \text{welding speed} - 7.17\ \text{voltage} \times \text{voltage} \\ & - 0.107\ \text{current} \times \text{current}\ 0.350\ \text{welding speed} \times \text{voltage} + 0.160\ \text{welding speed} \times \text{current} \\ & - 0.50\ \text{voltage} \times \text{current}.\end{aligned} \tag{1}$$

The coded coefficients were incorporated with various input factors with the P and T values. In this method weight was assigned to the input parameters in the range of <0.5. Therefore, this P value reaches the required positions, particularly the combinations of welding speed (0.260), current (0.302), and voltage and current (0.368). The coded coefficients of A-TIG process parameters were presented in Table 3. Similarly, Figure 4 exhibits the Pareto chart for

Table 3: Coded coefficients of flux-coated welded response by A-TIG.

Term	Coef	SE coef	*T*-value	*P*-value	VIF
Constant	263.33	8.03	32.79	0.001	
Welding speed	6.25	4.92	1.27	0.260	1.00
Voltage	2.50	4.92	0.51	0.633	1.00
Current	0.75	4.92	0.15	0.885	1.00
Welding speed × welding speed	−0.17	7.24	−0.02	0.983	1.01
Voltage × voltage	−7.17	7.24	−0.99	0.368	1.01
Current × current	−2.67	7.24	−0.37	0.728	1.01
Welding speed × voltage	−3.50	6.96	−0.50	0.636	1.00
Welding speed × current	8.00	6.96	1.15	0.302	1.00
Voltage × current	−2.50	6.96	−0.36	0.734	1.00

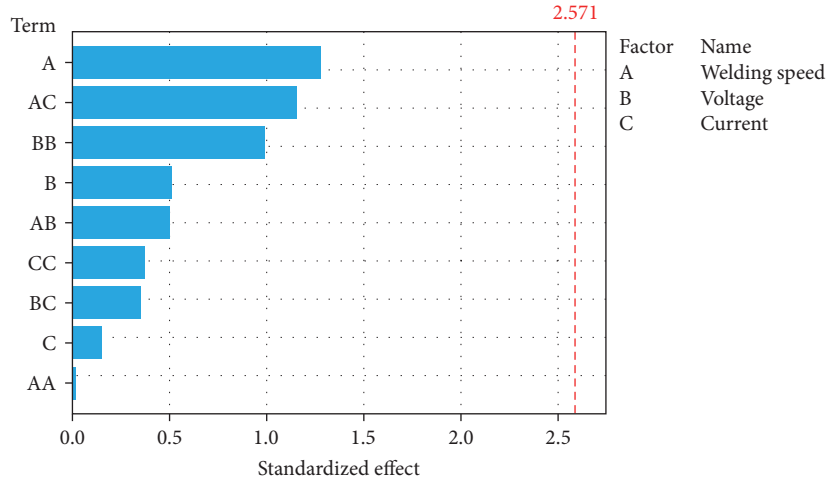

Figure 4: Standardized effect of Pareto chart for tensile strength.

tensile outcomes with normalized effects. From Figure 4, welding speed individual factor attained most level than other combinations of process parameters. The significant level was achieved in lesser level standardized effects of 1.5 limits. The ANOVA analysis was required to identify the significant level with various errors systems and the significant level was improved along with some processing parameters as discussed in the coefficients section. ANOVA creates significant factors for improving the characteristics of process parameters. Most of the parameters accomplished better significance. Table 4 displays the ANOVA for tensile outcomes with the input factors.

Regression equations build the model successfully with uncoded units for hardness response. The following equation displays the regression formulation for hardness strength.

$$\begin{aligned}\text{Hardness strength} = {} & -1379 + 5.66\ \text{welding speed} - 31.2\ \text{voltage} + 23.3\ \text{current} \\ & - 0.0158\ \text{welding speed} \times \text{welding speed} + 0.42\ \text{voltage} \times \text{voltage} \\ & - 0.0933\ \text{current} \times \text{current} + 0.000\ \text{welding speed} \times \text{voltage} \\ & - 0.0250\ \text{welding speed} \times \text{current} + 0.150\ \text{voltage} \times \text{current}.\end{aligned} \tag{2}$$

The coded coefficients of hardness response were incorporated with a choice of activated TIG factors with the *P* and *T* values. In this technique, weight basis was allotted to the input activated-TIG process parameters in the range (<0.5). Consequently, this *P* value performs the required ranking especially, the amalgamation of voltage (0.327), current (0.362), current × current (0.338), and welding speed and current (0.580) arrangements. The coded coefficients of A-TIG process parameters for hardness are shown in Table 5. Similarly, Figure 5 displays the Pareto chart for hardness outcome with standardized effects. From Figure 6, welding speed individual factor was accomplished most significant level than

Table 4: ANOVA for tensile output with their activated coated TIG parameters.

Basis	*df*	Adj. SS	Adj. MS	*F*-value	*P*-value
Model	9	904.33	100.481	0.52	0.815
Linear	3	367.00	122.333	0.63	0.625
Welding speed	1	312.50	312.500	1.61	0.260
Voltage	1	50.00	50.000	0.26	0.633
Current	1	4.50	4.500	0.02	0.885
Square	3	207.33	69.111	0.36	0.787
Welding speed × welding speed	1	0.10	0.103	0.00	0.983
Voltage × voltage	1	189.64	189.641	0.98	0.368
Current × current	1	26.26	26.256	0.14	0.728
Two-way interaction	3	330.00	110.000	0.57	0.660
Welding speed × voltage	1	49.00	49.000	0.25	0.636
Welding speed × current	1	256.00	256.000	1.32	0.302
Voltage × current	1	25.00	25.000	0.13	0.734
Error	5	967.67	193.533		
Lack-of-fit	3	351.00	117.000	0.38	0.782
Pure error	2	616.67	308.333		
Total	14	1,872.00			

Table 5: Coded coefficients for hardness response with various A-TIG process parameters.

Term	Coef	SE coef	*T*-value	*P*-value
Constant	87.67	2.44	35.91	0.001
Welding speed	−3.13	1.50	−2.09	0.091
Voltage	−1.62	1.50	−1.09	0.327
Current	−1.50	1.50	−1.00	0.362
Welding speed × welding speed	−1.58	2.20	−0.72	0.504
Voltage × voltage	0.42	2.20	0.19	0.857
Current × current	−2.33	2.20	−1.06	0.338
Welding speed × voltage	0.00	2.11	0.00	1.000
Welding speed × current	−1.25	2.11	−0.59	0.580
Voltage × current	0.75	2.11	0.35	0.737

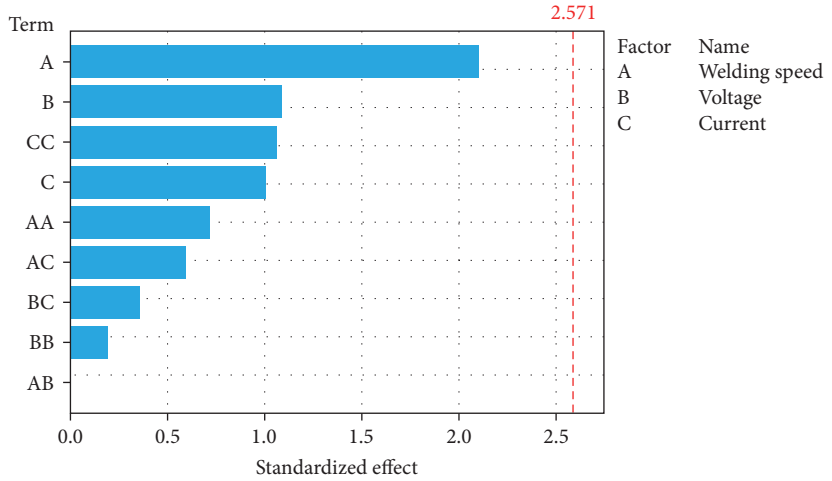

Figure 5: Standardized effect of Pareto chart for hardness strength.

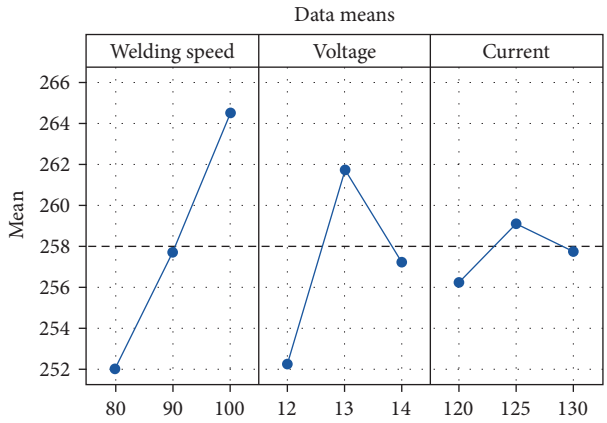

Figure 6: Main effect plot for tensile outcome with A-TIG-coated process samples.

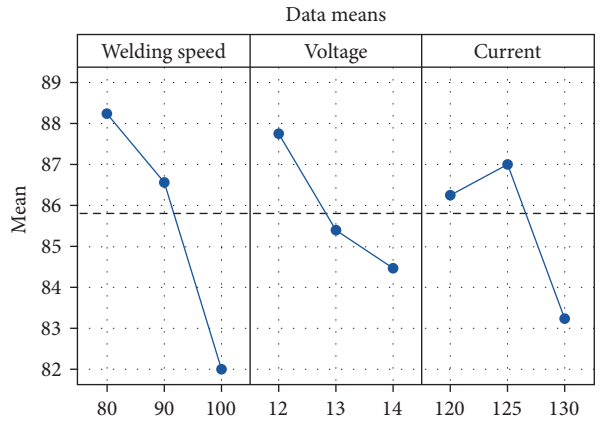

Figure 7: Main effect plot for hardness impact with A-TIG-coated process samples.

Table 6: ANOVA for hardness with their activated coated TIG parameters.

Source	*df*	Adj. SS	Adj. MS	*F*-value	*P*-value
Model	9	154.983	17.2204	0.96	0.549
Linear	3	117.250	39.0833	2.19	0.208
Welding speed	1	78.125	78.1250	4.37	0.091
Voltage	1	21.125	21.1250	1.18	0.327
Current	1	18.000	18.0000	1.01	0.362
Square	3	29.233	9.7444	0.54	0.673
Welding speed × welding speed	1	9.256	9.2564	0.52	0.504
Voltage × voltage	1	0.641	0.6410	0.04	0.857
Current × current	1	20.103	20.1026	1.12	0.338
2-way interaction	3	8.500	2.8333	0.16	0.920
Welding speed × voltage	1	0.000	0.0000	0.00	1.000
Welding speed × current	1	6.250	6.2500	0.35	0.580
Voltage × current	1	2.250	2.2500	0.13	0.737
Error	5	89.417	17.8833		
Lack-of-fit	3	22.750	7.5833	0.23	0.872
Pure error	2	66.667	33.3333		
Total	14	244.400			

the other combinations of A-TIG process parameters. The significant level was achieved in lesser level standardized effects of 2.0 limits.

The ANOVA was mandatory to recognize the noteworthy level with various errors system and the considerable level was enhanced along with some A-TIG processing parameters as conferred in the coefficients section. ANOVA produces significant factors for advancing the uniqueness of A-TIG process parameters. Most of the parameters proficient better significance. Table 6 shows the ANOVA for hardness outcomes with activated flux-coated TIG process input factors.

After the conclusion of ANOVA for both the responses tensile and hardness, further optimal values should be engaged to mean effect plots for enhancing the input parameters with combinational effects. Figure 6 displays the mean effect plot for tensile response with various A-TIG-coated process parameters. From these parameters, welding speed (100 mm/min), voltage (13 V), and current (125 amps) influenced the response to the next level so these parameters were optimal than the other TIG parameters.

Figure 7 exhibits the mean effect plot for hardness response with different A-TIG-coated process parameters. From these parameters, welding speed (80 mm/min), voltage (12 V), and current (125 amps) influenced the response to the next level so these parameters were optimal than the other TIG parameters. Compared with those mean effect plots both the processed parameters were attained efficiently, especially the current parameters on activated-nano-SiO_2 sample procures common factors for both the outcomes. During the TIG welding process, presence of nano-SiO_2 provides much adequate oxide levels in the welded region to remove the moisture gases and enhance the welded strength.

After mean effect plots, interaction effects were discussed in this part for the combinational arrangements for entire TIG process parameters to compose better joints among the AA5083-H111 specimens. Therefore, Figures 8 and 9 show

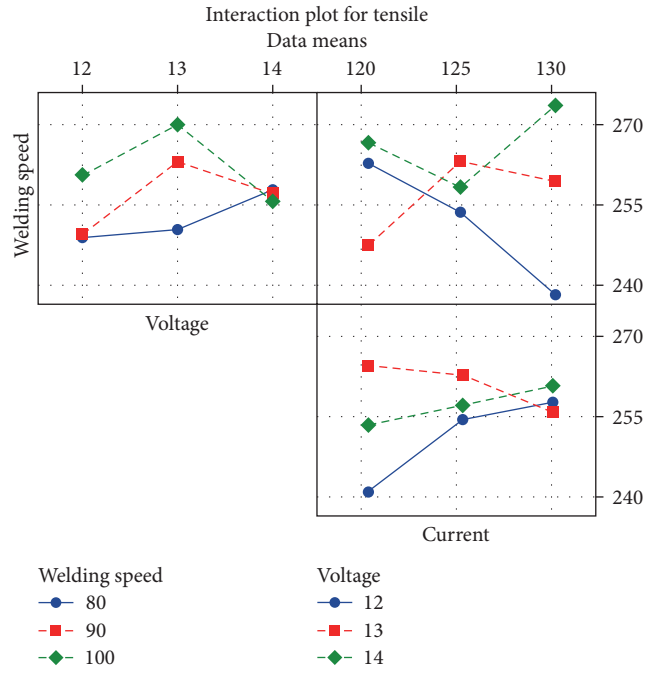

Figure 8: Interaction effect for tensile with A-TIG process on flux-coated welded AA5083.

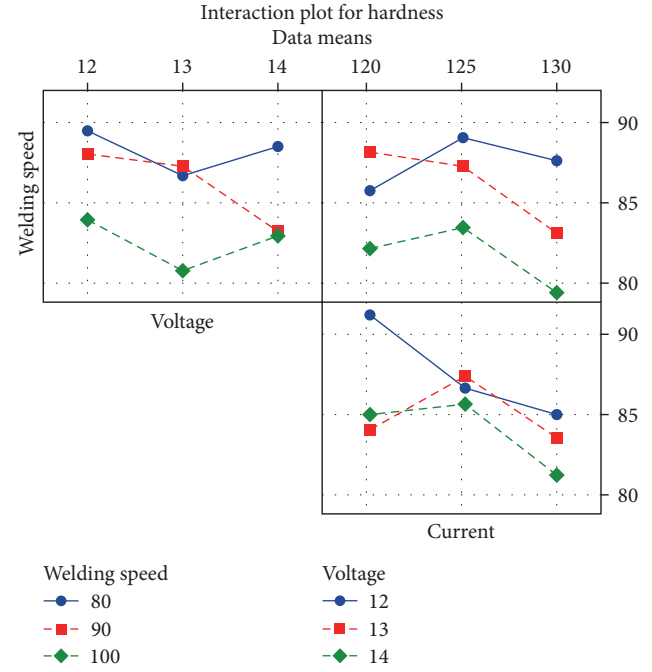

Figure 9: Interaction effect for hardness with A-TIG process on flux-coated welded AA5083.

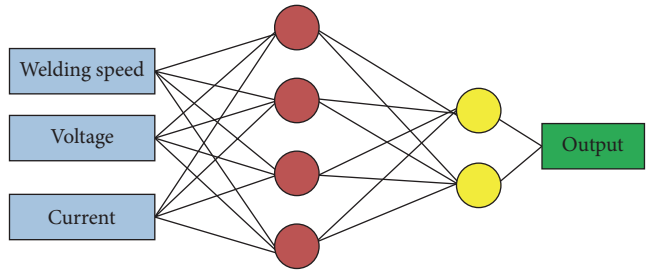

Figure 10: Neural network model for output responses with flux-coated welded AA5083.

Table 7: Predicted ANN for both coated welded outputs.

Weld order	Welding speed (mm/min)	Voltage (V)	Current (amp)	Tensile	ANN tensile	Hardness	ANN hardness
1	90	13	125	245	244.52	81	80.25
2	90	14	120	254	253.25	85	54.12
3	100	12	125	261	259.15	84	83.56
4	80	14	125	258	258.69	89	89.35
5	90	13	125	265	266.12	91	91.87
6	80	13	130	238	239.01	88	87.84
7	80	13	120	263	263.98	86	85.89
8	90	12	120	241	241.58	92	92.16
9	100	14	125	256	255.14	83	84.15
10	100	13	130	274	273.15	79	79.56
11	100	13	120	267	266.59	82	82.64
12	90	12	130	258	258.12	85	85.97
13	90	14	130	261	260.16	81	81.37
14	90	13	125	280	278.56	91	91.65
15	80	12	125	249	249.13	90	91.08

ANN, artificial neural network.

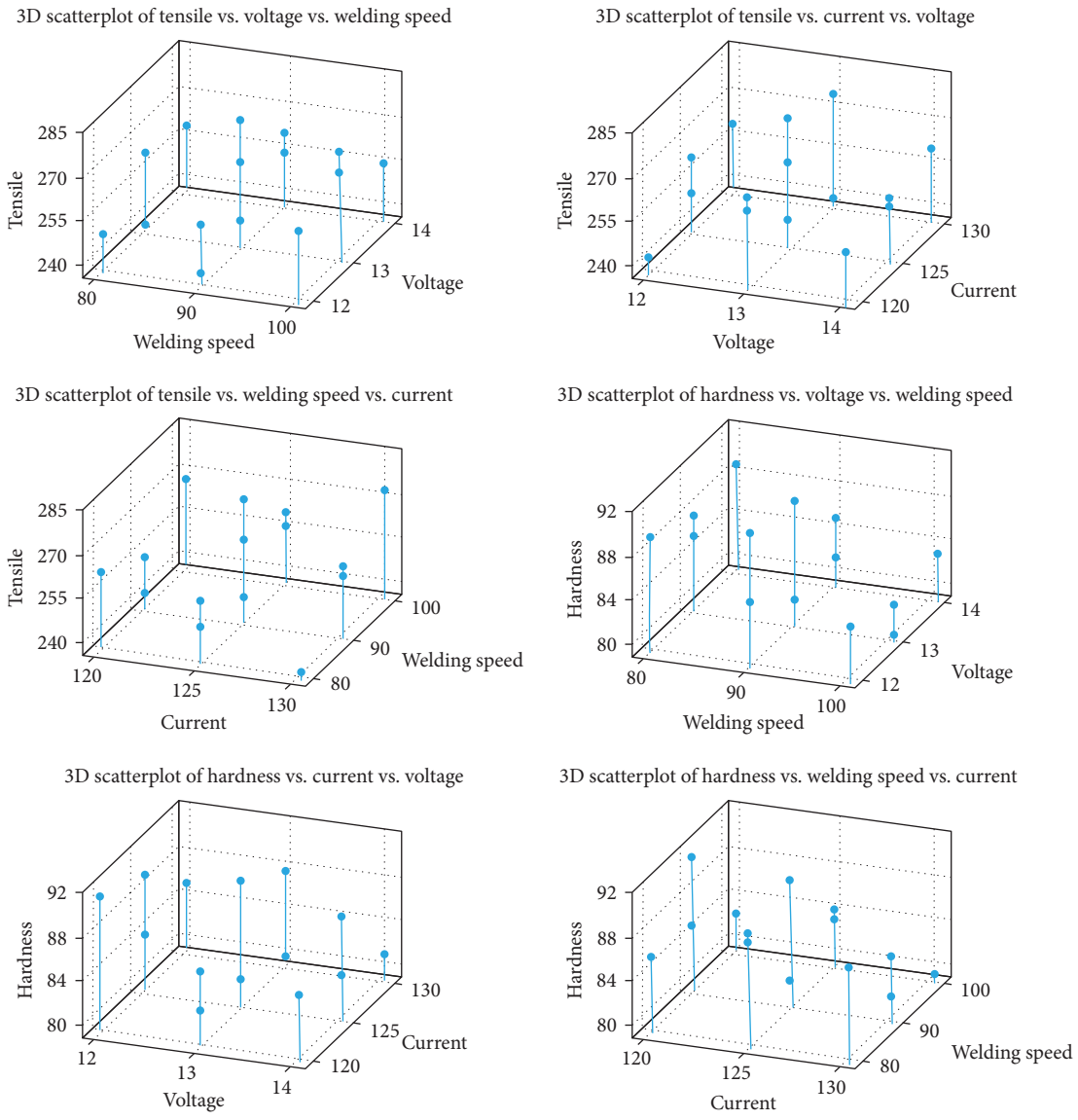

Figure 11: 3D scatter plot of output responses with activated TIG-flux-coated welded AA5083.

the interaction plots for tensile and hardness properties, respectively.

4. Neural Network Model for Predicting the Mechanical Responses

Neural network method was used to resolve the issues in more complicated responses. Therefore, neural network technique was created using the predicted values with appropriate weight basis process. Initially, the models were interconnected with various elements of training data with manipulation of weighted values. The real structure of neural network model was displayed in Figure 10. These networks values were bonded in proper way for each and every input factor that could lead to enhance the specified output responses. And the total sum of square responses were formed among the actual TIG-coated responses and predicted responses. Various researchers conducted numerous problems in the field of neural network method. In this research, Weka 3.8 software was utilized to compose the predicted response with selected A-TIG process parameters. In this technique, rate of learning, thrust, and hidden layers were the target and trial methods to maximize the coefficient of interrelations and to minimize the root mean square with error analysis. From the multilayer model with observation category, the predicted and investigational outputs were analyzed and are presented in Table 7. Table 7 predicts that artificial neural network (ANN) of output responses were enhanced effectively than the other investigational outcomes. Similarly, the 3D scatter plot also measured with experimental and predicted outcomes which fully relates with A-TIG-coated welded samples. Figure 11 shows the 3D scatter plot for output responses with various A-TIG-coated welded samples.

5. Conclusion

(1) The AA5083 and flux-coated nano-SiO_2 was synthesized successfully by the activated TIG welding process.

(2) The influence of nano-SiO_2 improves the welding strength with appropriate TIG process parameters.

(3) Process parameters were successfully optimized by Box–Behnken statistical method with the RSM technique.

(4) The output responses like tensile and hardness properties were enhanced effectively on the welded AA5083-H111.

(5) Due to the presence of nano-SiO_2 flux-coated optimum parameters, the optimal solution highly attains on sample 14 with a welding speed of 90 mm/min, voltage of 13 V, and current of 125 amps.

(6) Similarly, the regression analysis was utilized to analyze the parameters. Then the interaction plots and mean effects plots were successfully developed to improve the performances of process parameters.

(7) The ANOVA proves that the welding speed is the most influencing parameter than the other TIG welding parameters. The corresponding F value (0.09) of welding speed is less than other parameter values.

(8) Finally, the neural network approaches were influenced to observe the actual and predictable outcomes with support of 3D scatter plot.

(9) In the analysis of ANN, most of the outputs were improved by the predicted values and these process parameters were also validated with the ANOVA technique.

(10) The different particles categories like TiO_2, B4C, and chromium-based ceramic particles could be utilized in the upcoming research work.

Data Availability

The data used to support the findings of this study are included in the article. Should further data or information be required, these are available from the corresponding author upon request.

Conflicts of Interest

The authors declare that they have no conflicts of interest.

References

[1] D. Ren, Y. Jiang, X. Hu et al., "Investigation of tensile and high cycle fatigue failure behavior on a TIG welded titanium alloy," *Intermetallics*, vol. 132, Article ID 107115, 2021.

[2] A. Merneedi, L. Natrayan, S. Kaliappan et al., "Experimental investigation on mechanical properties of carbon nanotube-reinforced epoxy composites for automobile application," *Journal of Nanomaterials*, vol. 2021, Article ID 4937059, 7 pages, 2021.

[3] C. Meng, J. Yang, Z. Zhang et al., "Effect of laser bionic treatment on the microstructure and mechanical properties of TIG welded AZ31B magnesium alloy joints," *Materials Science and Engineering: A*, vol. 839, Article ID 142864, 2022.

[4] H. Rana, V. Badheka, P. Patel, V. Patel, W. Li, and J. Andersson, "Augmentation of weld penetration by flux assisted TIG welding and its distinct variants for oxygen free copper," *Journal of Materials Research and Technology*, vol. 10, pp. 138–151, 2021.

[5] L. Natrayan and M. S. Kumar, "Influence of silicon carbide on tribological behaviour of AA2024/Al_2O_3/SiC/Gr hybrid metal matrix squeeze cast composite using Taguchi technique," *Materials Research Express*, vol. 6, no. 12, Article ID 1265f9, 2019.

[6] V. Bhanu, A. Gupta, and C. Pandey, "Role of A-TIG process in joining of martensitic and austenitic steels for ultra-supercritical power plants—a state of the art review," *Nuclear Engineering and Technology*, vol. 54, no. 8, pp. 2755–2770, 2022.

[7] A. B. Zala, N. I. Jamnapara, C. S. Sasmal, S. Sam, and M. Ranjan, "Study of microstructure & mechanical properties of TIG welded aluminized 9Cr-1Mo steel," *Fusion Engineering and Design*, vol. 176, Article ID 113038, 2022.

[8] S. Yogeshwaran, R. Prabhu, L. Natrayan, and R. Murugan, "Mechanical properties of leaf ashes reinforced aluminum alloy

metal matrix composites," *International Journal of Applied Engineering Research*, vol. 10, no. 13, pp. 11048–11052, 2015.

[9] C. Meng, Z. Zhang, J. Yang, W. Zhuang, and H. Shi, "Effect of laser bionic treatment on fatigue crack growth behavior of TIG welded AZ31B magnesium alloy joint," *Materials Letters*, vol. 320, Article ID 132334, 2022.

[10] M. S. Kumar, L. Natrayan, R. D. Hemanth, K. Annamalai, and E. Karthick, "Experimental investigations on mechanical and microstructural properties of Al_2O_3/SiC reinforced hybrid metal matrix composite," *IOP Conference Series: Materials Science and Engineering*, vol. 402, Article ID 012123, 2018.

[11] A. K. Unni and M. Vasudevan, "Numerical modelling of fluid flow and weld penetration in activated TIG welding," *Materials Today: Proceedings*, vol. 27, Part 3, pp. 2768–2773, 2020.

[12] P. Sharma and D. K. Dwivedi, "Improving the strength-ductility synergy and impact toughness of dissimilar martensitic–austenitic steel joints by A-TIG welding with wire feed," *Materials Letters*, vol. 285, Article ID 129063, 2021.

[13] K.-H. Tseng and C.-Y. Hsu, "Performance of activated TIG process in austenitic stainless steel welds," *Journal of Materials Processing Technology*, vol. 211, no. 3, pp. 503–512, 2011.

[14] S. Chai, S. Zhong, Q. Yang et al., "Transformation of laves phases and its effect on the mechanical properties of TIG welded Mg–Al–Ca–Mn alloys," *Journal of Materials Science & Technology*, vol. 120, pp. 108–117, 2022.

[15] A. R. Pavan, N. Chandrasekar, B. Arivazhagan, S. Kumar, and M. Vasudevan, "Study of arc characteristics using varying shielding gas and optimization of activated-TIG welding technique for thick AISI 316L(N) plates," *CIRP Journal of Manufacturing Science and Technology*, vol. 35, pp. 675–690, 2021.

[16] A. Babbar, A. Kumar, V. Jain, and D. Gupta, "Enhancement of activated tungsten inert gas (A-TIG) welding using multi-component TiO_2–SiO_2–Al_2O_3 hybrid flux," *Measurement*, vol. 148, Article ID 106912, 2019.

[17] T. Sakthivel, M. Vasudevan, K. Laha et al., "Comparison of creep rupture behaviour of type 316L(N) austenitic stainless steel joints welded by TIG and activated TIG welding processes," *Materials Science and Engineering: A*, vol. 528, no. 22-23, pp. 6971–6980, 2011.

[18] M. Muzamil, J. Wu, M. Akhtar, V. Patel, A. Majeed, and J. Yang, "Multicomponent enabled MWCNTs-TiO_2 nano-activating flux for controlling the geometrical behavior of modified TIG welding joint process," *Diamond and Related Materials*, vol. 97, Article ID 107442, 2019.

[19] J. J. Vora and V. J. Badheka, "Experimental investigation on microstructure and mechanical properties of activated TIG welded reduced activation ferritic/martensitic steel joints," *Journal of Manufacturing Processes*, vol. 25, pp. 85–93, 2017.

[20] J. Wu, Z. Wang, S. Lin et al., "Effect of fast-frequency pulsed waveforms on the microstructure and mechanical properties of Ti–6Al–4V alloy welded by FFP-TIG," *Journal of Materials Research and Technology*, vol. 20, pp. 516–531, 2022.

[21] L. Natrayan, R. Anand, and S. Santhosh Kumar, "Optimization of process parameters in TIG welding of AISI 4140 stainless steel using Taguchi technique," *Materials Today: Proceedings*, vol. 37, Part 2, pp. 1550–1553, 2021.

[22] J. Zhang, Y. Huang, D. Fan et al., "Microstructure and performances of dissimilar joints between 12Cr2Mo1R steel and 06Cr18Ni11Ti austenitic stainless steel joined by AA-TIG welding," *Journal of Manufacturing Processes*, vol. 60, pp. 96–106, 2020.

[23] A. Baghel, C. Sharma, S. Rathee, and M. Srivastava, "Activated flux TIG welding of dissimilar SS202 and SS304 alloys: effect of oxide and chloride fluxes on microstructure and mechanical properties of joints," *Materials Today: Proceedings*, vol. 47, Part 19, pp. 7189–7195, 2021.

[24] G. Qin, C. Feng, and H. Ma, "Suppression mechanism of weld appearance defects in tandem TIG welding by numerical modeling," *Journal of Materials Research and Technology*, vol. 14, pp. 160–173, 2021.

[25] B. Qin, F.-C. Yin, C.-Z. Zeng, J.-C. Xie, and J. Shen, "Microstructure and mechanical properties of TIG/A-TIG welded AZ61/ZK60 magnesium alloy joints," *Transactions of Nonferrous Metals Society of China*, vol. 29, no. 9, pp. 1864–1872, 2019.